TISSUE ENGINEERING: Part A
Volume 19, Numbers 15 and 16, 2013

DOI: 10.1089/ten.tea.2012.0694

Modulating the Behaviors of Mesenchymal Stem Cells Via the Combination of High-Frequency Vibratory Stimulations and Fibrous Scaffolds

Zhixiang Tong, BS,[1] Randall L. Duncan, PhD,[2–4] and Xinqiao Jia, PhD[1,2,4]

We are interested in the *in vitro* engineering of artificial vocal fold tissues via the strategic combination of multipotent mesenchymal stem cells (MSCs), physiologically relevant mechanical stimulations, and biomimetic artificial matrices. We have constructed a vocal fold bioreactor that is capable of imposing vibratory stimulations on the cultured cells at human phonation frequencies. Separately, fibrous poly (ε-caprolactone) (PCL) scaffolds emulating the ligamentous structure of the vocal fold were prepared by electrospinning, were incorporated in the vocal fold bioreactor, and were driven into a wave-like motion in an axisymmetrical fashion by the oscillating air. MSC-laden PCL scaffolds were subjected to vibrations at 200 Hz with a normal center displacement of ~40 μm for a total of 7 days. A continuous (CT) or a 1 h-on-1 h-off (OF) regime with a total dynamic culture time of 12 h per day was applied. The dynamic loading did not cause any physiological trauma to the cells. Immunohistotochemical staining revealed the reinforcement of the actin filament and the enhancement of $\alpha_5\beta_1$ integrin expression under selected dynamic culture conditions. Cellular expression of essential vocal fold extracellular matrix components, such as elastin, hyaluronic acid, and matrix metalloproteinase-1, was significantly elevated as compared with the static controls, and the OF regime is more conducive to matrix production than the CT vibration mode. Analyses of genes of typical fibroblast hallmarks (tenascin-C, collagen III, and procollagen I) as well as markers for MSC differentiation into nonfibroblastic lineages confirmed MSCs' adaptation of fibroblastic behaviors. Overall, the high-frequency vibratory stimulation, when combined with a synthetic fibrous scaffold, serves as a potent modulator of MSC functions. The novel bioreactor system presented here, as a versatile, yet well-controlled model, offers an *in vitro* platform for understanding vibration-induced mechanotransduction and for engineering of functional vocal fold tissues.

Introduction

Human vocal fold, composed of a stratified squamous epithelium, the lamina propria (LP), and the vocalis muscle, is a specialized soft tissue that converts aerodynamic energy into acoustic waves for sound production.[1] During normal phonation, vocal folds oscillate regularly at strains up to 30% in a broad range of frequencies (100–300 Hz).[2] Histologically, adult LP is divided into superficial (SLP), intermediate (ILP), and deep (DLP) layers. The epithelium and the SLP combined constitute the mucosa layer, while the ILP and DLP are referred to as the vocal ligament.[3] The SLP consists primarily of an amorphous matrix, sparsely decorated with loose fibers, whereas the vocal ligament is rich in collagen and elastin that entangle into a micro-fibrous network to provide tensile strength to the tissue.[4] Being the major type of cells in the vocal fold LP, fibroblasts are responsible for maintaining the tissue homeostasis.[3] Newborn and mature vocal folds are distinctly different in terms of their matrix composition, structural organization, and tissue biomechanics. Although the mechanism governing vocal fold maturation is not yet well understood, it has been proposed that the vocalization-derived mechanical stimuli and local hormone receptors may be the contributing factors.[5–8]

Numerous conditions, such as voice abuse, allergies, intubation, or surgeries, can disrupt the vibratory structures of the LP and compromise the tissue pliability, giving rise to vocal fold dysfunction that affects an estimated 3%–9% of the population.[9] Current treatments for vocal fold disorders usually involve voice therapy, repetitive therapeutic injections, or surgical procedures.[10] These approaches may be effective in improving voice quality temporarily. However, long-term, functional tissue regeneration has not yet been achieved. Mesenchymal stem cell (MSC)-based regenerative strategy is emerging as a promising alternative treatment option for the restoration of functional vocal folds owing to

[1]Department of Materials Science and Engineering, Delaware Biotechnology Institute, University of Delaware, Newark, Delaware.
Departments of [2]Biological Sciences, [3]Mechanical Engineering, and [4]Biomedical Engineering Program, University of Delaware, Newark, Delaware.

their multipotency, self-renewal capability, and clinical availability.[11] Moreover, studies have shown that primary vocal fold fibroblasts (PVFFs) and MSCs share similar cell surface markers, immunophenotypic characteristics, and differentiation potential.[12] Thus, MSCs are a suitable alternative to PVFFs for vocal fold tissue engineering. MSCs are naturally sensitive to their environment, and each tissue contains a unique stem cell niche that fosters the tissue-specific stem cell differentiation and tissue development.[13] In addition to the biochemical environment, biomechanical forces have been shown to be potent regulators of cell fate and are necessary for tissue development, function, and homeostasis.[14,15] It has been demonstrated that physiologically relevant mechanical stimuli can guide stem cell differentiation and accelerate tissue-specific matrix remodeling for a variety of tissue engineering applications.[16–19]

Titze and coworkers developed a vocal fold bioreactor[20] that integrates a static stretch with a high-frequency (20–200 Hz) oscillation to stimulate cellular production of matrix proteins. Employing this bioreactor design, Webb and coworkers[21] investigated the temporal patterns of gene expression and matrix deposition by human dermal fibroblasts encapsulated in hyaluronic acid (HA)-based hydrogels and exposed to 100 Hz vibrations for 10 days. Compared with the static controls, dynamically cultivated cell/gel constructs exhibited elevated levels of mRNA for HA synthase 2 (*HAS2*), decorin, fibromodulin, and matrix metalloproteinase-1 (*MMP1*) in a time-dependent fashion. Enhanced accumulation of sulfated glycosaminoglycans and decreased production of collagen were also observed after 10 days of dynamic culture. A similar device has been utilized to compare the responses of PVFFs and MSCs, entrapped in microporous Tecoflex® elastomer, with high-frequency vibration stimulations.[22] Recently, Farran *et al.*[23] created a dynamic cell culture device using a power amplifier, a function generator, an enclosed loud speaker, and a circumferentially anchored silicon membrane. The vibration signals were translated to the membrane aerodynamically by the oscillating air pressure underneath. Neonatal foreskin fibroblasts attached to the membrane were subjected to a 1 h vibration at 60, 110, and 300 Hz, with the displacement at the center of the membrane varying in the range 1–30 μm, followed by a 6 h rest. Quantitative polymerase chain reaction (qPCR) results showed that the expression of genes encoding some extracellular matrix (ECM) proteins was moderately altered in response to changes in vibratory frequency and amplitude.

Overall, successful engineering of vocal fold LP requires the strategic combination of multipotent MSCs, biomimetic matrices, and physiologically relevant biomechanical stimulations.[24] In the current study, we designed and constructed a novel dynamic cell culture device that was capable of generating phonation-mimicking vibrations without evoking any physiological trauma to MSCs cultured in an electrospun fibrous scaffold. Microfibrous poly(ε-caprolactone) (PCL) scaffolds were employed to recapitulate the structure of the vocal fold ligament. MSC-populated PCL scaffolds were incorporated into the device and exposed to 200 Hz sinusoidal vibrations for 7 days. Different vibration regimes, namely continuously 12 h or 1 h-on-1 h-off for a total of 12 h daily, were introduced and the dynamic effects were compared. Cellular responses, in terms of cell proliferation, cell morphology, and the expression of vocal fold-relevant ECM genes and proteins, were investigated systematically. Overall, MSCs residing in fibrous PCL scaffolds responded to the high-frequency vibratory stimulations via an integrin-mediated process that resulted in a profound alteration of their matrix production.

Materials and Methods

Scaffold fabrication and characterization

Fibrous PCL scaffolds were fabricated using a conventional electrospinning setup.[25] Briefly, a chloroform (Sigma Aldrich) solution (16 wt%) of PCL (Sigma Aldrich; $M_n \sim 80$ kDa) was loaded into a 10 mL syringe that was capped with a 21G blunt ended needle (Becton Dickinson). The syringe was locked onto a programmable syringe pump (New Era Pump Systems), and the flow rate was set at 1 mL/h. The voltage between the syringe needle and the ground aluminum foil placed 18 cm from the needle tip was maintained at 15 kV. Fibers were allowed to accumulate on the aluminum collector to a thickness of ~250–300 μm, and the resultant scaffolds were stored in a vacuum desiccator for 1–2 days to remove any residual solvent. PCL scaffolds were imaged using a scanning electron microscope (SEM, JSM-7400F; JEOL-USA) after being sputter coated with gold (Denton Vacuum Desk). The fiber diameter was analyzed using Image J (NIH, 99) software. To facilitate cell attachment, the scaffolds were soaked in a fibronectin (FN; Sigma Aldrich) solution (20 μg/mL in PBS) at 37°C for 1 h. The FN-coated scaffolds were stained with mouse-derived fibronectin antibody, followed by Alexa-488 conjugated rabbit anti-mouse IgG before being imaged with an LSM 5 Live high-speed confocal microscope (Zeiss). Scaffolds without the FN coating and staining experiments without using FN antibody were included to confirm the specificity of the antibody reaction.

Bioreactor design

The bioreactor consists of two aluminum alloy bars (1, Fig. 1A), each housing four parallel vibration chambers (2, Fig. 1A), a function generator (3, Fig. 1A), a power amplifier (4, Fig. 1A), and a speaker selector (5, Fig. 1A). The vibration chamber was created by sandwiching a custom-made silicone disk (1, Fig. 1B) between a pair of acrylic blocks (2, and 3, Fig 1B) with a circular opening (Ø = 24 mm) in the middle. The top (1.8 cm thick) and bottom (0.9 cm thick) acrylic blocks were engraved with a matching ridge and groove to hold the elastomeric disk in place. Four corner screws were employed to connect the paired blocks, creating a water- and air-tight vibration chamber that was 24 mm wide and 18 mm deep. The silicone disk (Ø = 42 mm, thickness = 1.2 mm) was prefabricated with an entrenched sleeve (Ø = 12 mm, thickness = ~250 μm) in the middle, through which a fibrous PCL scaffold (4 in Fig. 1B, C) was conveniently inserted and securely locked in (insert, Fig. 1A). The silicone disk also served as the bottom of the cell culture chamber. A Sony speaker (5, Fig. 1B, 8 Ω/11 W) was anchored directly underneath the vibration chamber through another four corner screws on the bottom acrylic block. The speakers were controlled individually by a speaker selector (RadioShack) and driven by a function generator (Agilent 33220A; Agilent) through a power amplifier (Pyle Pro PT-2400). The oscillating

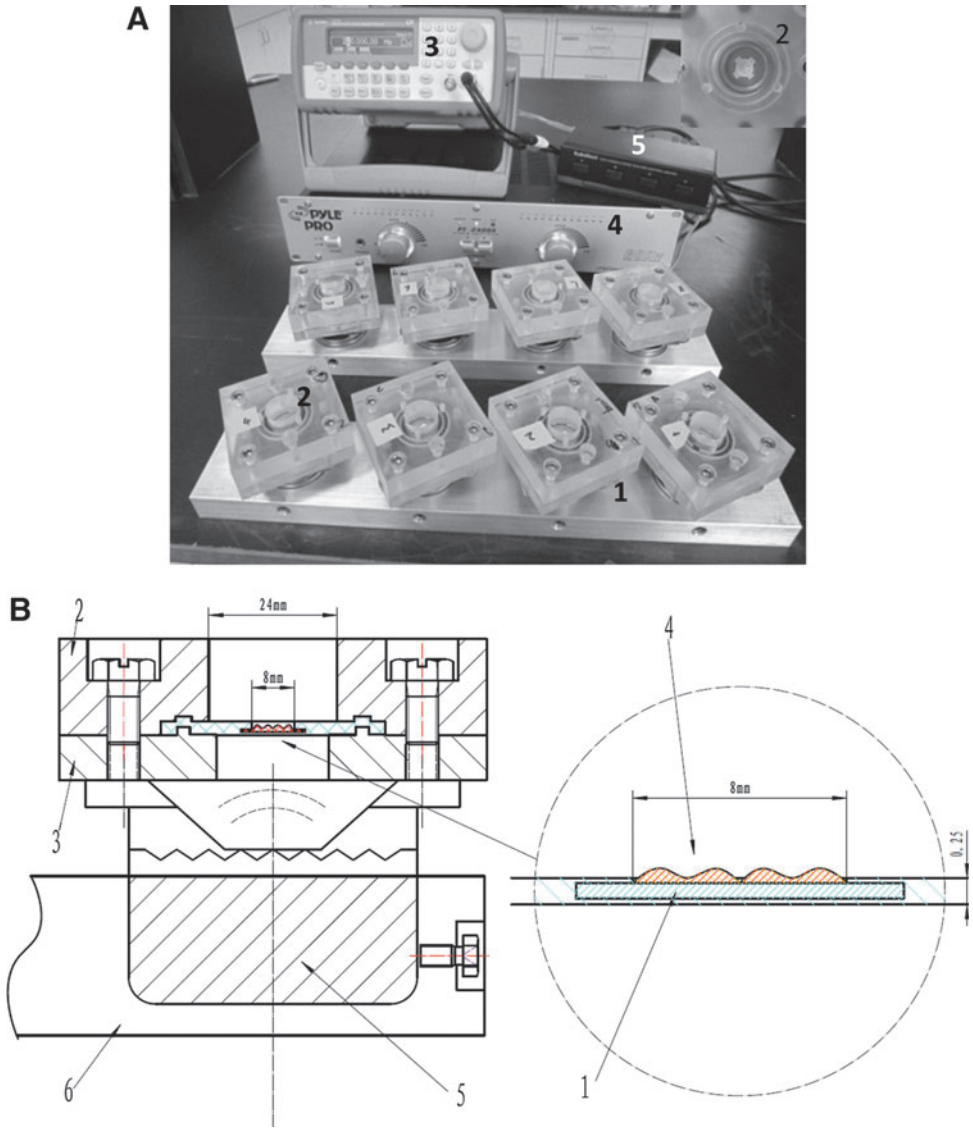

FIG. 1. A custom-designed vocal fold bioreactor. **(A)** A digital picture showing the major components of the bioreactor. 1: Al platform; 2: vibration chamber; 3: function generator; 4: power amplifier; 5: speaker selector. The insert at the top-right corner shows the top view of a vibration chamber (2) with a poly (ε-caprolactone) (PCL) scaffold held in place. **(B)** A cross-sectional view of a vibration chamber. 1: silicone disk (cyan); 2 top acrylic plate; 3: bottom acrylic plate; 4: PCL scaffold (red); 5: loud speaker; 6: Al platform. Color images available online at www.liebertpub.com/tea

air pressure, generated by the vibrating speaker cone, was transmitted to the scaffold/disk assembly aerodynamically. Four individual vibration chambers were affixed to each stationary alloy bar (1 in Fig. 1A and 6 in Fig. 1B). The resulting chamber array was duplicated so that a total of eight vibration chambers were included in the system. The two chamber arrays, speaker selector, and associated electronic wires were encased in an anti-humidity acrylic box housed inside a commercial incubator, while the function generator and power amplifier were placed outside. The main cable linking the power amplifier and speaker selector was fed through the filter assembly at the back of the incubator. The opening of the vibration chambers was covered with a sterile, microporous adhesive film (Denville Scientific) to allow for free exchange of O_2/CO_2 during cell culture.

Bioreactor characterization

A single-point Laser Doppler Vibrometer (LDV) was employed to quantify the vibration signals received by the silicone disk and the PCL scaffold in the presence of water (1.5 mL). Specifically, the laser was focused perpendicularly at a predetermined point on the selected substrate, and the reflected beam was received and processed by the vibrometer (PDV-100; Polytec). The signals were further analyzed by the VibSoft data acquisition software (Polytec) to obtain information on the vibration frequency (*f*), normal displacement (w), velocity (v), and acceleration (a). Single-point analysis at different radial positions of the silicone disk or the PCL scaffold allowed for the construction of a vibration profile across the substrate. A 3D colormap correlating the vibratory profile, in terms of the normal displacement, across the substrate was generated using the Origin 8.5 software (OriginLab Corp.).

Cell culture and dynamic treatments

Primary human bone marrow mesenchymal stem cells (Lonza) were sub-cultured at a seeding density of 4000–5000 cells/cm^2 on a T150 tissue culture flask (Corning) in MSC maintenance media (Lonza). After reaching ~80% confluence, MSCs (passages 3–5) were trypsinized, centrifuged, and

re-suspended in fresh MSC media. Separately, the PCL scaffolds were sterilized in 70% ethanol overnight, followed by a 15-min exposure to a bactericidal UV lamp. The sterile scaffolds were then coated with fibronectin and were subsequently inserted into the silicone disk. The bioreactor was assembled just before cell seeding. The cell suspension (4.5 million cells/mL, total of 40 μL) was evenly pipetted onto the scaffolds, and cells were allowed to attach for 1.5 h before the MSC maintenance media (1.5 mL) were added. The cell-laden scaffolds were precultured statically for 3 days before the vibration was introduced. Initial cell viability and attachment were confirmed by live/dead staining and F-actin/vinculin co-staining, respectively, following the procedures previously described.[19] Sinusoidal vibrations at 200 Hz with a normal displacement of ~40 μm at the center of the scaffold (w_0) were imposed on the constructs for 7 days either continuously for 12 h per day (referred to as CT culture) or discontinuously in a 1 h-on-1 h-off pattern for a total of 12 h daily (referred to as OF culture). Identical acrylic chambers housing the same cellular constructs and cultured in a separate incubator without vibration served as the static controls (referred to as ST culture). Medium was refreshed every other day. To simplify the discussion, the end of the initial 3 days of preculture is designated as day 0 for the following dynamic culture. After 0, 3, and 7 days of vibrations, the cellular constructs and cell culture supernatants were collected separately for further biological evaluations.

Biological evaluations

Metabolic activity, viability, and proliferation. Cellular metabolic activity was monitored by Alamar blue cell viability assay (Invitrogen). To this end, cells were cultured dynamically in the presence of Alamar blue for 2.5 h before medium refreshment every other day. Subsequently, the medium (100 μL) was aliquoted into a 96-well plate, and the fluorescence intensity was detected (Ex/Em: 550/590 nm) using a microplate reader (Perkin-Elmer). In addition, cell viability after 7 days of dynamic culture was confirmed by live/dead staining followed by confocal fluorescence imaging. Specifically, the cellular constructs were rinsed with cold Dulbecco's phosphate-buffered saline (DPBS; Gibco), stained with propidium iodide (1:2000 in DPBS; Invitrogen) and Syto-13 (1:1000 in DPBS; Invitrogen) for 5 min, and imaged with a multiphoton confocal microscope (Zeiss 510 NLO). Finally, DNA content per scaffold was quantified by Picogreen DNA assay (Invitrogen) after scaffold digestion following a previously reported procedure.[19] Briefly, the constructs were snap frozen on dry ice and digested with 0.2 mg/mL papain (Sigma Aldrich) in 0.2 M sodium phosphate buffer (pH 6.4) at 65°C for 2–3 h.[19] After removing the insoluble scaffold debris by centrifugation, digestion aliquots (100 μL) and DNA standards were used for DNA quantification following the manufacturer's instruction.

F-actin and Integrin $\alpha_5\beta_1$ immuno-staining. The cellular constructs were rinsed with cold DPBS and then fixed with 4% paraformaldehyde (Electron Microscopy Science) in DPBS for 15 min on ice. The constructs were then permeabilized with 0.1% Triton X-100 solution in DPBS for 5 min on ice, washed twice with DPBS, and blocked with 3% bovine serum albumin (BSA; Jackson Immuno Research) for 40 min at ambient temperature. Afterward, samples were incubated with integrin $\alpha_5\beta_1$ primary antibody (mouse-derived monoclonal; Abcam) at a 1:200 dilution in 1% BSA overnight at 4°C. After repetitive washing (three times) with DPBS containing 0.05% Tween-20 (Fisher), the constructs were incubated with Alexa-488 goat anti–mouse IgG (1:200 dilution with 1% BSA; Invitrogen) and TRITC-conjugated Phalloidin (Millipore; 1:400 in 1% BSA) for 1 h in the dark. Finally, the scaffolds were counterstained with DAPI (1:1000 in DPBS; Millipore) for 10 min, and imaged with the confocal microscope. To semi-quantitatively assess the F-actin and integrin expression, Z-stacked images (within 50 μm thickness of scanning) were analyzed by Volocity 3D-4D imaging analysis software (Perkin Elmer).

Gene expression analysis. Immediately after the completion of the dynamic culture, the constructs were briefly rinsed with cold DPBS, snap frozen on dry ice, and crushed using a tissue pestle (Fisher) in the presence of 1 mL Trizol reagent (Invitrogen). After complete dissociation, chloroform (0.2 mL) was added to the homogenized digestion, and the mixture was agitated for 10 min, followed by centrifugation at 14,000 rpm for 15 min at 4°C. Subsequently, the total RNA and proteins were extracted from different layers of the phase-separated digestion mixture, following the procedure described elsewhere.[19] The quality and quantity of the purified RNA samples were verified using a Nanodrop ND-2000 Spectrophotometer (NanoDrop Products). The isolated RNA from each sample was reverse transcribed into cDNA using a QuantiTect reverse transcription kit (Qiagen). qPCR was performed on an ABI 7300 real-time sequence detection system using SYBR green PCR master mix (Applied Biosystems), using the thermal cycling program previously reported.[19] Specifically, the qPCR was carried out with a reaction volume of 25 μL containing 5 ng cDNA, 12.5 μL SYBR Green PCR master mix (2×), and 1 μL primer mix. Sequences of the reverse and forward primers for the genes involved in this study are listed in Table 1. All primers were synthesized by Integrated DNA technologies. To ensure the robustness of qPCR data analysis, multiple reference genes (*YWHAZ*, *TBP*, and *PPIA*, refer to Table 1) were employed as the internal controls, and the variation of specific primer efficiencies was taken into account.[26–28] Relative expression (fold change) of the genes of interest from the vibrated samples was calibrated by the geometric mean of the three reference genes, and further normalized against that of the respective static controls at corresponding time points.[29] This data analysis process was performed using the qbasePLUS software (Biogazelle).[30]

Biochemical analysis. The production of HA, tenascin-C (TNC), MMP-1, and elastin (ELN) at the protein level was quantified by biochemical assays. Aliquots (200 μL) of the cell culture supernatants collected every other day after the vibrations were pooled together until day 7 (800 μL total per sample). These samples were aliquoted and diluted accordingly for different enzyme-linked immunosorbent assays (ELISA). Specifically, the HA secreted into the medium was quantified using a competitive HA ELISA kit (Echelon Biosciences). Soluble tenascin-C (high-molecular-weight variant) production was assayed with a solid phase

Table 1. Summary of the Quantitative Polymerase Chain Reaction Primer Information

Gene	*Forward primer (5′-3′)*	*Reverse primer (5′-3′)*	*GenBank #*	*Product size (bp)*	*Efficiency*
ProCol I α1[59]	AATGGTGCTCCTGGTATTGCTGGT	ACCAGTGTCTCCTTTGCTGCCA	NM_000088	141	2.10
ELN[19]	AAAGCAGCAGCAAAGTTCGG	ACCTGGGAC AACTGGAATCC	NM_001081755	288	1.99
FN[23]	ACCTACGGATGACTCGTGCTTTGA	CAAAGCCTAAGCACTGGCACAACA	NM_002026	116	2.10
DCN[19]	GATGCAGCTAGC CTGAAAGG	TCACACCCGAATAAGAAGCC	NM_133503	274	1.98
MMP1 [23]	GGGAGATCATCGGGACAACTC	GGGCCTGGTTGAAAAGCAT	NM_002421	72	2.03
Col3A1[60]	TGGTGCCCCTGGTCCTTGCT	TACGGGGCAAAACCGCCAGC	NM_000090	87	2.03
HAS3[19]	TGTGCAGTGTATTAGTGGGCCCTT	TTGGAGCGCGTATACTTAGTT	NM_005329	177	1.90
HAS1[61]	GTGAGTGGCTGTACAACGCG	AGAGGGACGTAGTTAGCGGC	NM_001523	355	1.91
LOX[62]	GCGCTGTGACATTCGCTACA	GCTTTGCCTTCTAATACGGTGAA	NM_002317	77	2.00
ITGA5[63]	GTCGGGGGCTTCAACTTAGAC	CCTGGCTGGCTGGTATTAGC	NM_002205	152	1.99
COX2[64]	GCCCAGCACTTCACGCATCAG	AGACCAGGCACCAGACCAAAGACC	NM_000963	290	1.92
αSMA[65]	CCAAGCACTGTCAGGAAT	AGGCAGTGCTGTCCTCTT	NM_001613	60	1.99
TNC	GGGCTGGTTGTATTGATGCTTT	AGGGACCACTGGGTGAGAGA	NM_002160	76	2.00
FSP1[19]	AGCTTCTTGGGGAAAAGGAC	CCCCAACCACAT CAGAGG	NM_019554	200	1.98
aP2[66]	AACCTTAGATGGGGGTGTCCTG	TCGTGGAAGTGACGCCTTTC	NM_001442	125	2.10
ALP[11]	GCCTACCAGCTCATGCATAAC	GAAGTGGGAGTGCTTGTATCT	NM_000478	192	2.07
ACAN[19]	TCGAGGACAGCGAGGCC	TCGAGGGTGTAGCGTGTAGAGA	NM_013227	85	2.03
p53[19]	TGCGTGTGGAGTATTTGGATG	GTGTGATGATGGTGAGGATGG	NM_000546	168	2.05
YWHAZ[67]	TGCTTGCATCCCACAGACTA	AGGCAGACAATGACAGACCA	NM_003406	126	2.00
PPIA[63]	GGCAAATGCTGGACCCAACAC	TGCCATTCCTGGACCCAAAGC	NM_021130	152	2.08
TBP[68]	TGCACAGGAGCCAAGAGTGAA	CACATCACAGCTCCCCACCA	NM_003194	132	2.07

Primer sequences for TNC were designed based on gene sequence obtained from GenBank (NM_002160) using Primer 3 software (http://frodo.wi.mit.edu/primer3/). All the other sequences were obtained from published records.

Gene symbols: ProCol I α1, procollagen I alpha 1 chain; ELN, elastin; FN, fibronectin; DCN, decorin; Col3A1, collagen III alpha 1 chain; MMP1, matrix metalloproteinase-1; HAS1, hyaluronan synthase 1; HAS3, hyaluronan synthase 3; LOX, lysyl oxidase; ITGA5, integrin alpha 5 unit; COX2, cyclooxygenase-2; αSMA, alpha smooth muscle actin; TNC, tenascin-C; FSP1, fibroblast specific protein-1; aP2, adipocyte Protein 2; ALP, alkaline phosphatase; ACAN, aggrecan; YWHAZ, tyrosine 3-monooxygenase/tryptophan 5-monooxygenase activation protein, zeta polypeptide; PPIA, peptidylprolyl isomerase A; TBP, TATA-binding protein.

sandwich ELISA kit (Immuno-Biological Laboratories). Total MMP1 secretion was evaluated using an MMP1 DuoSet ELISA Development kit (R&D systems). The production of cross-linked elastin and soluble elastin precursor (tropoelastin) was examined separately. To quantify the insoluble elastin, the total protein extraction obtained from Trizol/chloroform digestion (detailed above) was boiled with 0.25 M oxalic acid (Sigma Aldrich), following the previous procedure.[19] Afterward, the solubilized elastin extracts were assayed using a Fastin elastin assay kit (Biocolor). Tropoelastin was quantified via a previously established ELISA protocol with minor modifications.[31] Specifically, a high-binding EIA/RIA plate (Corning) was incubated with 100 μL of media samples (diluted by a factor of 10 with 50 mM pH 9.6 bicarbonate coating buffer containing 0.02% NaN_3; Sigma) and α-elastin standards (Biocolor, 5, 4, 3, 2, 1, and 0 μg/mL in coating buffer) at 4°C overnight. The plate was washed thrice with DPBS, and blocked with 3% BSA for 2 h at room temperature. The bound elastin antigen was detected with BA4 mouse anti-elastin primary antibody (Sigma Aldrich; 1:1000 dilution with 1% BSA in DPBS) for 2 h at room temperature. After thorough rinsing with wash buffer (DPBS containing 0.05% Tween-20), the plate was incubated with 1:5000 (in 1% BSA) polyclonal rabbit anti-mouse IgG conjugated with horseradish peroxidase (HRP; Abcam) for 1 h. Subsequently, the color was developed by reacting HRP with a substrate reagent pack (R&D Systems) containing equal volumes of 3,3′,5,5′-tetramethylbenzidine and H_2O_2 for 20 min. Finally, the color development was quenched by adding 50 μL 2 N H_2SO_4 (Fisher), and its absorbance was detected using a PerkinElmer microplate reader at 450 nm with the background correction at 570 nm.

Statistical analysis

Unless otherwise noted, all quantitative data were reported as the mean ± standard error of the mean (SEM) from at least three parallel repeats. Student's two-tailed t test was used to determine the significant differences between groups, where $p < 0.05$ was considered statistically different.

Results

In the current study, we have constructed a novel dynamic cell culture device that is capable of mimicking the mechanical environment of human vocal folds during normal phonation. It has been successfully characterized using a single-point LDV in a noncontact and nondestructive fashion. Fibrous PCL scaffolds were fabricated and validated to support the attachment and growth of MSCs. The PCL scaffolds containing attached MSCs were driven into oscillation in an axisymmetrical fashion. Cells were subjected to static (ST), continuous (CT), or on-and-off (OF) treatment for 7 days, and cellular responses were evaluated at the transcriptional and translational levels by qPCR analyses and biochemical assays, respectively.

Characterization of PCL scaffolds

The electrospun PCL scaffolds displayed a random fiber orientation and a homogeneous fiber entanglement (Fig. 2A).

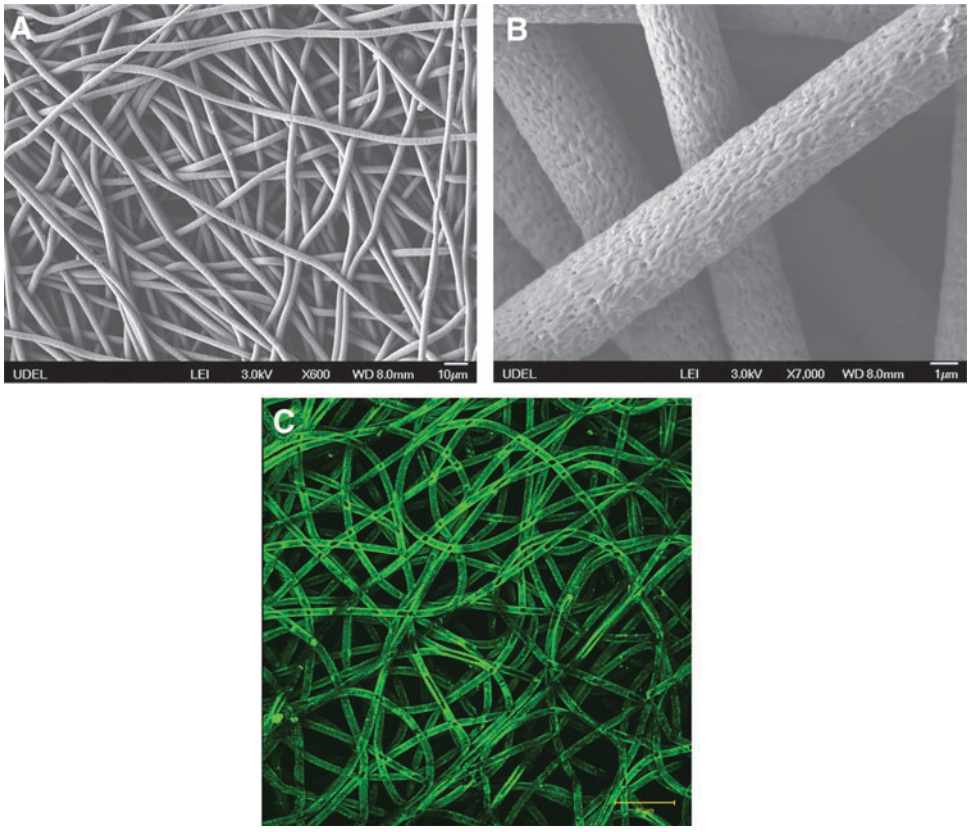

FIG. 2. Characterization of PCL scaffolds in terms of the microstructure **(A, B)** and fibronectin adsorption **(C)**. **(A, B)** SEM images of PCL scaffold at different magnifications. **(C)** Immunostaining confirming the fibronectin (green) retention on the PCL fibers after the scaffold was immersed in a fibronectin solution for 1 h. Color images available online at www.liebertpub.com/tea

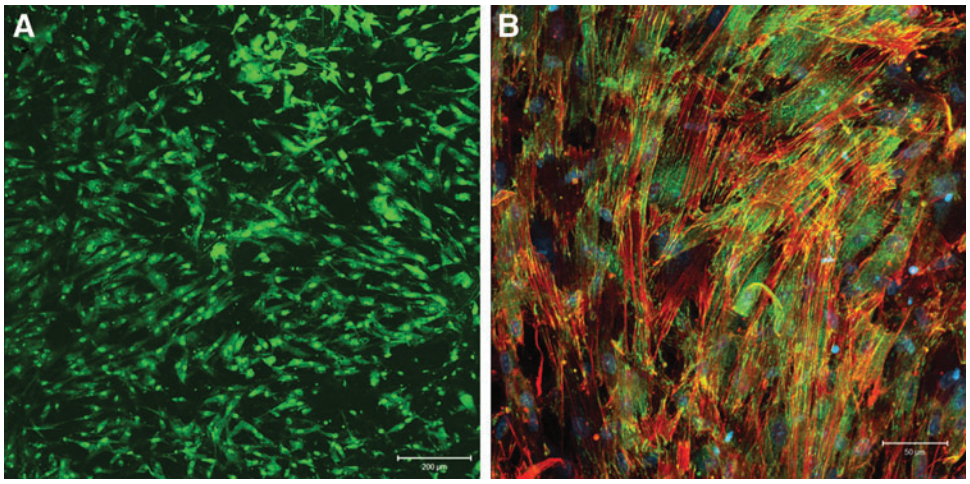

FIG. 3. Characterization of PCL scaffolds in terms of their capability to support mesenchymal stem cells (MSCs) attachment and growth. **(A)** Representative live/dead staining of MSCs after 3 days of preculture on/in the PCL scaffolds. Live (green) and dead cells (red) were stained with Syto13 and propidium iodine, respectively. **(B)** Representative F-actin/vinculin co-staining of MSCs after 3 days of preculture. F-actin (red) was stained by TRITC-phalloidin, focal adhesion sites (green) were stained by anti-vinculin, and FITC-conjugated secondary antibody, and nuclei (blue) were counterstained by Draq5. Color images available online at www.liebertpub.com/tea

The average fiber diameter was $4.7 \pm 0.5\,\mu m$, and the interstitial pores are micron sized, comparable to the dimension of MSCs. Inspection of the higher magnification image of the PCL scaffolds (Fig. 2B) revealed that the fiber surface was not smooth, but displayed nanoscale topography (grooves and pores). Scaffolds with a thickness $\sim 250\,\mu m$ were utilized for cell culture studies. Immersing the scaffolds in a fibronectin solution for 1 h resulted in a significant fibronectin retention on/in the fibers (Fig. 2C). Live/dead staining results indicate that the cells evenly populated the scaffold during the initial 3-day preculture (Fig. 3A). Three days post seeding, cells readily spread out, developed well-defined stress fibers (red stain in Fig. 3B), and adopted an elongated morphology on the fibers. Intense vinculin staining (green dots) was detected at the tail region of the F-actin, suggesting the formation of focal adhesion complex between the cells and the fibrous substrate.[31] On completion of the 3-day preculture, the cell-laden scaffolds were subjected to selected dynamic culture conditions (CT or OF) for approximately 7 days (see below). Throughout the entire culture period, under both static and dynamic conditions, the cell-laden scaffolds maintained their overall shape and size. In addition, MSCs subjected to 7-day CT culture conditions penetrated $\sim 100\,\mu m$ into the scaffolds (data not shown).

Bioreactor characterization

The bioreactor contains 8 vibration chambers that were individually driven by an underlying loud speaker. A sinusoidal wave, with desired frequency (f) and peak-to-peak voltage (V_{pp}), was introduced to the speakers via the speaker selector (5, Fig.1A). The oscillating air flow created between the paper cone of the speaker and the bottom of the silicone disk was delivered to the cellular scaffold (insert, Fig.1A) secured in the vibration chamber. Laser Doppler Vibrometry (LDV) was used to monitor the vibration characteristics of the silicone disk under the conditions employed for dynamic cell culture studies, taking into consideration the refractive index of water (1.33).[32] Figure 4 shows the normal displacement at the center of the disk (w_0) as a function of the driving frequency and voltage. The driving frequency was fixed at 100, 200, and 300 Hz, corresponding to the fundamental speaking frequencies of adult men, adult women, and children, respectively.[33] Overall, w_0 is a linear function of V_{pp} in the range of 0–1.0 V at all three frequencies tested. At any given output voltage, as f increased from 100 Hz to 300 Hz, the w_0 value decreased accordingly.

The vibration at 200 Hz with a V_{pp} of 0.8 V was selected for further characterization and subsequent dynamic cell culture. The velocity profile as a function of time (Supplementary Fig. S1A; Supplementary Data are available online

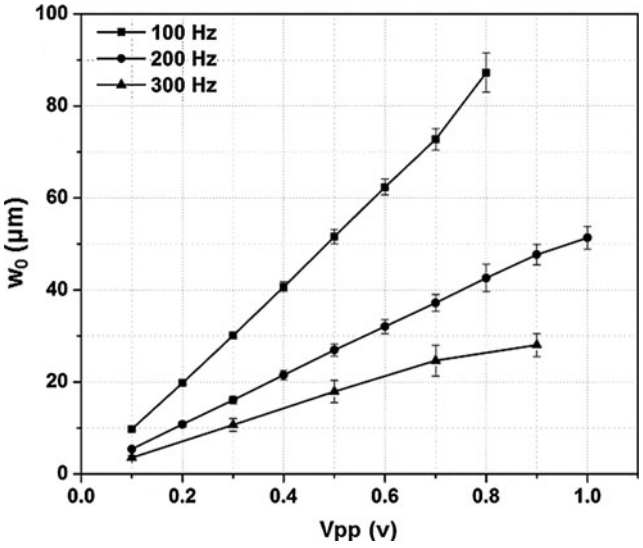

FIG. 4. The normal displacement at the center of the silicone disk (w_0) as a function of the applied frequency (100, 200 and 300 Hz) and the driving voltage (Vpp = 0–1 V).

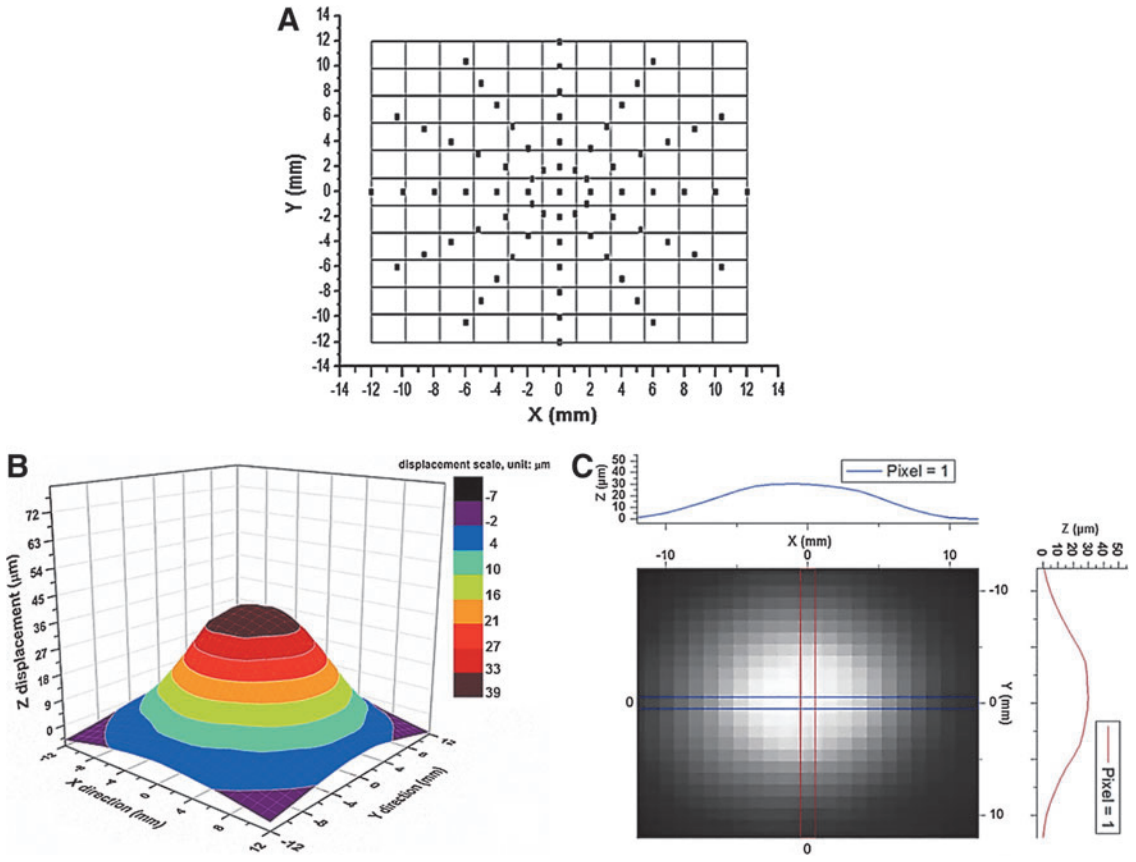

FIG. 5. 3D mapping of the vibration profile of the silicone disk at a frequency of 200 Hz and a driving voltage of 0.8 V. **(A)** Selected locations of the silicone disk marked for single-point Laser Doppler Vibrometer (LDV) measurements. **(B)** 3D colormap constructed by surface gridding using the normal displacement data collected from all locations marked on the disk. **(C)** Profile image of the colormap showing the symmetry of the vibration in representative orthogonal directions. Grayscale displays the variation of the normal displacement on the disk, with the brightest region representing the maximum displacement in the middle of the disk. Color images available online at www.liebertpub.com/tea

at www.liebertpub.com/tea) shows that the input sinusoidal signal was captured by the silicone disk with high fidelity. The center of the disk oscillates longitudinally at a peak velocity of 52.1 mm/s (Supplementary Fig. S1B), a peak acceleration of 65.5 m/s^2 (6.7g, Supplementary Fig. S1C), and a normal displacement of 41 μm (Supplementary Fig. S1D). In addition to the fundamental peak at 200 Hz, harmonic signals at 100, 300, 400, and 500 Hz (Supplementary Fig. S1B–D) were also present, but their amplitudes were at least one order of magnitude lower than those at the fundamental frequencies. The vibration pattern across the disk was constructed by measuring the normal displacement from a total of 73 representative points on the radial directions of the disk (Fig. 5A). The 3D colormap image (Fig. 5B) illustrates that the vibration detected at the disk is axisymmetric with regard to the center of the disk as well as its resting position. The detected z-displacement decreased monotonically from the center to the edge. This vibration pattern was further confirmed by the profile view of the z-displacement across two pairs of parallel lines in orthogonal directions (Fig. 5C) on the disk. For the dynamic culture studies, a vibration frequency of 200 Hz was selected to represent the average fundamental speaking frequency of male and female adults. A V_{pp} of 0.8 V was chosen to obtain the highest normal displacement with the least interference from the harmonic signals and liquid perturbation that could complicate our data interpretation.

Dynamic culture of MSCs in fibrous scaffolds

In this study, MSCs were employed in place of PVFFs for *in vitro* engineering of vocal fold tissues, owing to MSCs' self-renewal capability, multi-potency, and superior availability to PVFFs.[11] The dynamic culture device, combined with the microfibrous scaffold, established a vocal fold-like microenvironment that guides MSCs to produce vocal fold-like ECM.

Cellular viability, metabolic activity, and proliferation. Figure 6A shows the metabolic activity of MSCs cultured statically or dynamically at various times normalized to the initial day 0 level. Although the cellular metabolism was moderately ($p < 0.05$) decreased for MSCs cultured under OF conditions as compared with the static controls at day 4, Alarmar blue assay did not reveal any significant difference for cells under ST, CT, and OF conditions at day 6. Overall, cellular metabolic activity for all the experimental groups was significantly ($p < 0.05$) enhanced compared with day 0. Similarly, the DNA content per construct (Fig. 6B) did not vary significantly among different experimental groups.

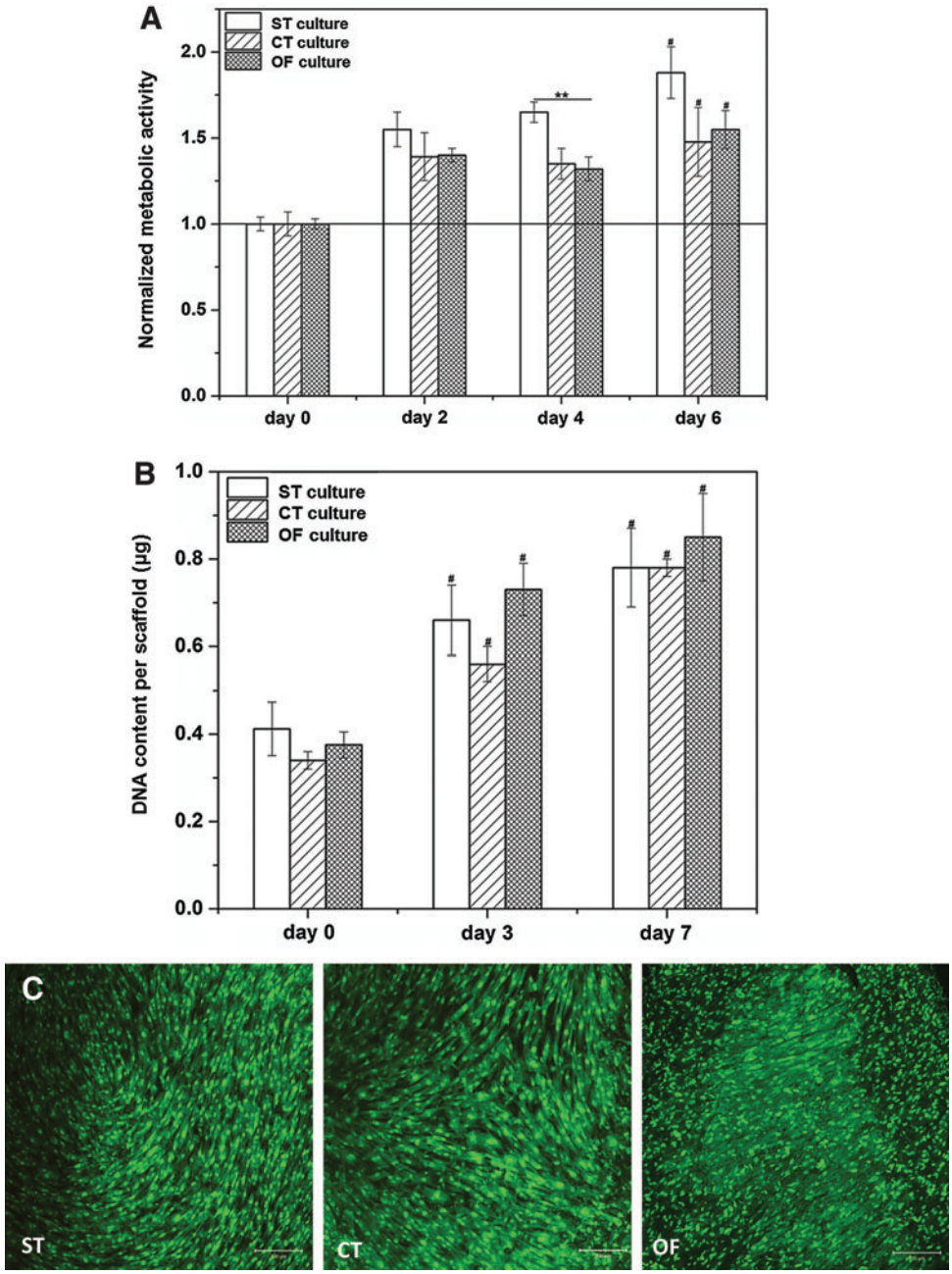

FIG. 6. Effects of vibratory stimulations on MSCs in terms of the metabolic activity and cell proliferation. **(A)** Cellular metabolic activity examined by alamar Blue assay, the respective fluorescence signals were normalized to the initial baseline level after the 3 day preculture before the initiation of the dynamic culture (day 0). **(B)** Cell proliferation, as revealed by picogreen DNA assay, during 7 days of dynamic culture. **(C)** Cell viability (visualized by live/dead staining) under different culture conditions at day 7. Scale bar: 200 μm. **significant difference ($p < 0.05$) between ST and OF vibration conditions; #significantly elevated ($p < 0.05$) relative to the initial day 0 level. Color images available online at www.liebertpub.com/tea

MSCs proliferated by ~2.5-fold ($p < 0.01$) at day 7 relative to day 0 for all respective cultures. Live/dead cell viability staining (Fig. 6C) revealed a similar density of viable cells in all the scaffolds after 7 days of vibrations, further confirming the cytocompatible nature of the fibrous scaffold and the nondestructive nature of the dynamic culture conditions employed.

Actin filament reinforcement and integrin $\alpha_5\beta_1$ expression. Integrin and actin cytoskeleton play an indispensable role in cell-matrix interaction and mechanotransduction.[34] Our F-actin staining results (Fig. 7A) show that cells adopted an elongated, spindle shape and maintained fibroblast-like morphology. After 7 days of dynamic culture, the F-actin filaments reorganized and clustered into dense bundles in the dynamically cultivated cells, in sharp contrast to the individual, well-separated filaments with a relatively weak staining seen in the static controls. The immunostaining of integrin $\alpha_5\beta_1$ revealed a more intense staining for CT samples than for OF samples or ST controls. Semi-quantitative image analyses (Fig. 7B) confirm the reinforcement of F-actin filaments for dynamic cultures. Compared with the static controls, F-actin staining for CT and OF cultures was 1.46 ± 0.09 ($p < 0.001$) and 1.40 ± 0.21 ($p < 0.02$) folds stronger, respectively. Integrin $\alpha_5\beta_1$ expressed by cells exposed to the 7-day CT conditions was significantly higher ($p < 0.001$) than static controls (1.31 ± 0.09-fold). Cells subjected to OF conditions did not exhibit a significant enhancement in integrin expression relative to the static cultures.

Cellular response at the mRNA level. Cellular responses to vibratory stimulations were examined at the mRNA level

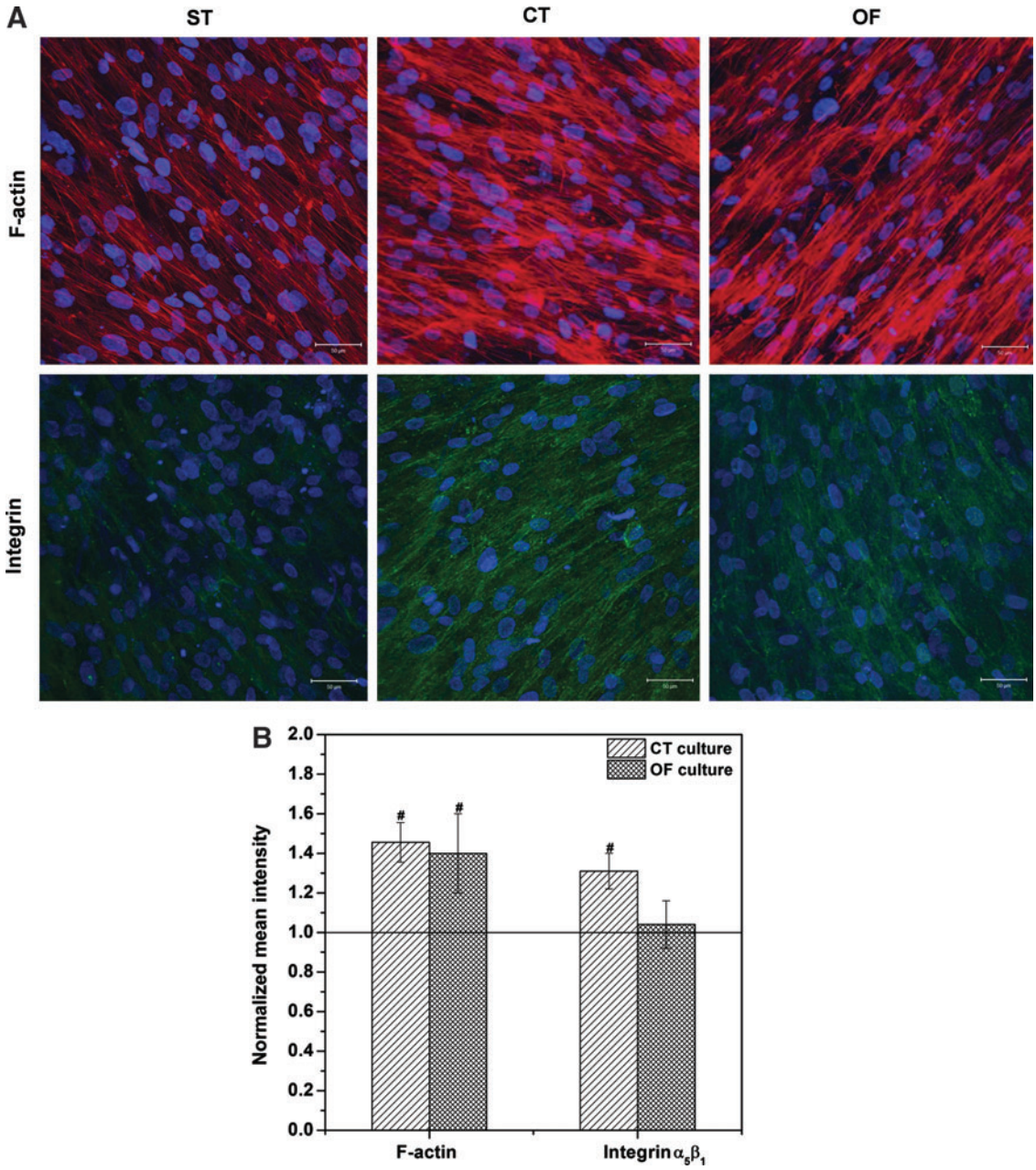

FIG. 7. Effects of vibratory stimulations on MSCs in terms of the expression of F-actin filament and integrin $\alpha_5\beta_1$ **(A)**. F-actin (red), integrin (green), and nuclei (blue) were stained by Alexa-568 phalloidin, Alexa-488 conjugated antibody, and DAPI, respectively. Scale bar: 50 μm. Images were obtained by merging z-stack slices over 50 μm scanning depth. Semi-quantitative image analysis **(B)** was performed by normalizing the mean intensity (green or red channel) of the unit image area to that of the static controls. Data were acquired from representative images from 3–4 independent trials (7–12 images each trial). #significantly ($p<0.05$) enhanced relative to the static controls (baseline). Color images available online at www.liebertpub.com/tea

by qPCR. First, the dynamic effects on the expression of genes encoding essential vocal fold ECM components, such as fibronectin (*FN*), elastin (*ELN*), decorin (*DCN*), collagen III αI (*Col3A1*), and procollagen I (*ProCol I*), were analyzed (Fig. 8A). Compared with static controls, the 3-day CT treatment significantly ($p<0.001$) attenuated the expression of *FN* and *DCN*. On the other hand, the 3-day OF treatment did not induce any significant changes in *FN* and *DCN* expression relative to the static baseline. For both genes, their relative expression was statistically higher ($p=0.01$) at day 7 for CT cultures than at day 3. Such a temporal effect was not observed under the OF conditions. It should be noted that a 7-day OF culture regime resulted in a significant increase in *FN* expression, with a 1.14 ± 0.04-fold increase relative to the static controls ($p=0.03$) and a 1.16 ± 0.03-fold increase ($p=0.02$) relative to the 7-day CT cultures.

The relative expression of *ELN* was found to be strikingly up-regulated after 7 days of dynamic culture, with a 1.58 ± 0.12 and 2.34 ± 0.38-fold increase relative to the static controls for CT and OF cultures, respectively. The up-

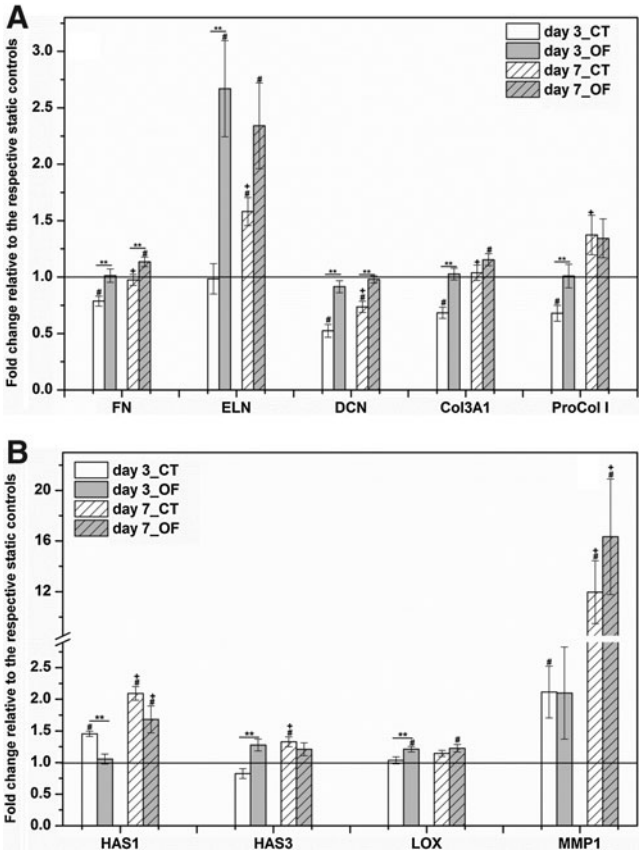

FIG. 8. Effects of vibratory stimulations on MSCs in terms of the expression of extracellular matrix (ECM)-related genes. **(A)** Quantitative polymerase chain reaction (qPCR) analyses of genes encoding essential vocal fold ECMs: *FN*, *ELN*, *DCN*, *Col3A1*, and *ProCol I*. **(B)** qPCR analyses of genes encoding typical ECM remodeling enzymes: *HAS1*, *HAS3*, *LOX*, and *MMP1*. The relative gene expression (fold change) was normalized to the respective static controls at day 3 and day 7 (baseline). **significant difference ($p < 0.05$) between CT and OF vibrations, #significantly changed ($p < 0.05$) relative to the respective static controls, +significantly different ($p < 0.05$) between day 3 and day 7 under corresponding vibration mode.

regulation of *ELN* expression occurred earlier for the OF cultures (day 3) than the CT cultures. *ELN* expression by cells cultured under CT conditions was significantly ($p = 0.004$) elevated from day 3 to day 7. Cells vibrated intermittently in an OF fashion expressed a significantly higher ($p < 0.001$) level of *Col3A1* than those exposed to a CT vibration for 3 days. However, such a difference was attenuated when cells were vibrated for 7 days. Compared with the static controls, the dynamic 3-day CT treatment led to a significant decrease ($p = 0.015$) in the expression of *ProCol I*. *ProCol I* expression was elevated, on average, by 1.4 fold for both CT and OF cultures at day 7, with the CT samples exhibiting a significant ($p = 0.003$) enhancement at day 7 compared with day 3.

Next, four crucial ECM remodeling enzymes, HA synthase 1 (*HAS1*), HA synthase 3 (*HAS3*), lysyl oxidase (*LOX*), and *MMP1*, were examined by qPCR (Fig. 8B). Both the OF and the CT treatments significantly up-regulated the *HAS1* expression, with a 2.09 ± 0.11 and 1.68 ± 0.21-fold increase compared with the static controls at day 7, respectively. Under both conditions, the stimulatory effect was more pronounced when the treatment was prolonged beyond day 3. Overall, the CT mode was more efficacious ($p < 0.001$) than the OF regime in promoting *HAS1* expression at day 3. Similarly, relative *HAS3* expression at day 7 under CT conditions (1.33 ± 0.08-fold, $p = 0.01$) was remarkably elevated ($p < 0.001$) compared with the day 3 level (0.82 ± 0.08-fold). However, the mRNA level of *HAS3* was not statistically altered after 7 days of OF culture. When compared with the respective static controls, the mRNA level of *LOX* in OF samples was distinctly increased at day 3 (1.21 ± 0.04-fold, $p = 0.01$) and day 7 (1.23 ± 0.06-fold, $p = 0.002$). Moreover, at day 3, *LOX* expression under OF conditions was significantly higher ($p = 0.02$) than that of the CT cultures. The mRNA level *MMP1* was remarkably up-regulated on CT (12 ± 2.5-fold, $p = 0.0001$) and OF treatments (16.3 ± 4.6-fold, $p = 0.001$) at day 7. The dynamic CT treatment induced an earlier response at day 3, with a fold change relative to the corresponding static controls of 2.11 ± 0.41 ($p = 0.03$). Furthermore, the inductive effect of the high-frequency vibration on *MMP1* gene expression was significantly ($p < 0.02$) enhanced from day 3 to day 7, under both vibration modes.

In addition, putative mechano-responsive genes, such as tenascin-C (*TNC*), *COX2*, integrin α_5 (*ITGA5*), and *p53*, were evaluated by qPCR (Fig. 9A). Except for the 3-day CT treatment, all other dynamic conditions (3-day-OF, 7-day-CT, 7-day-OF) up-regulated the expression of *TNC* compared with the static counterparts. A 7-day vibratory stimulation gave rise to a significant ($p < 0.0001$) increase in the *TNC* expression relative to the static controls (1.26 ± 0.06 for CT treatment and 1.41 ± 0.05 for OF treatment). For *COX2*, 3-day treatment did not result in any significant alteration in its expression. However, prolonging the OF treatment to 7 days led to a profound increase of *COX2* expression (2.09 ± 0.25-fold, ($p = 0.0001$) relative to the static controls. The 7-day CT regime also led to an up-regulation of *COX2* (1.36 ± 0.15-fold, $p = 0.0001$), although this change was distinctly lower ($p = 0.007$) than that induced by the 7-day OF treatment. Our qPCR results revealed that *ITGA5* is highly sensitive to high-frequency vibratory stimulations. A 7-day CT treatment gave rise to a fold increase of 2.47 ± 0.23 compared with the static controls, whereas a 7-day OF vibration resulted in a 2.26 ± 0.32-fold enhancement, both of which were significantly higher than the corresponding 3-day regimes. Of note, the dynamic vibration conditions applied did not cause any significant change in the expression of *p53*.

Finally, genes encoding classic MSC differentiation markers (Fig. 9B), including α-smooth muscle actin (*αSMA*), fibroblast specific protein-1 (*FSP1*), aggrecan (*ACAN*), alkaline phosphate (*ALP*), and adipocyte Protein 2 (*aP2*), were systematically characterized. No significant difference was observed for *αSMA* expression between the static and the 7-day CT cultures. However, the expression of *αSMA* was significantly elevated (1.95 ± 0.25-fold, $p = 0.005$) after 3 day OF treatment. This fold increase was drastically attenuated ($p = 0.002$) and leveled off by day 7. With regard to *FSP1*, its relative expression was stable around the baseline level from day 3 to day 7 under both vibration modes, and a moderate suppression (0.82 ± 0.05-fold, $p = 0.02$) was detected after 3 days of OF culture. Dynamic culture only slightly modulated the expression of a chondrogenesis marker, *ACAN*, above the

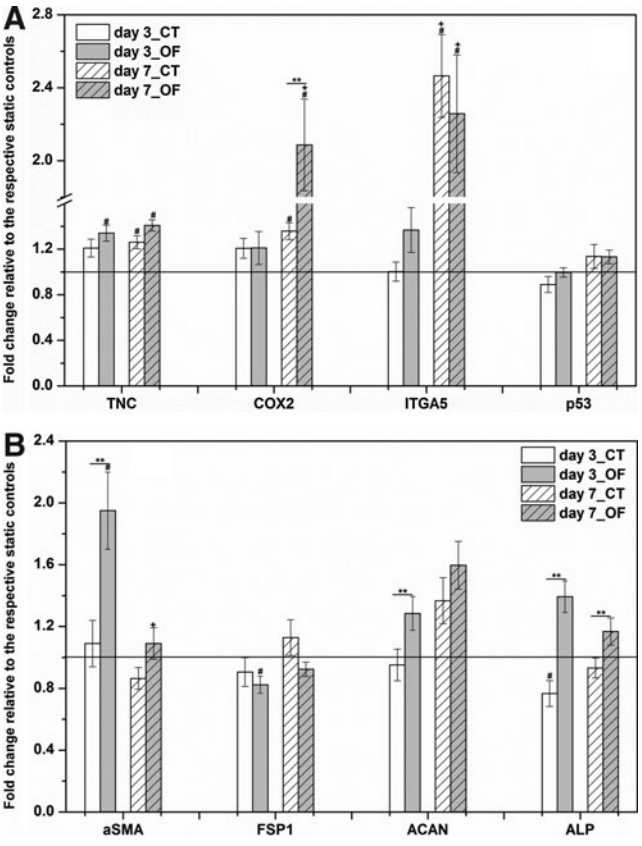

FIG. 9. Effects of vibratory stimulations on MSCs in terms of the expression of mechanosensitive genes and marker genes. **(A)** Genes encoding putative mechanosensitive molecules: *TNC*, *COX2*, *ITGA5*, and *p53*. **(B)** Genes encoding classic MSCs differentiation markers: α*SMA*, *FSP1*, *ACAN*, and *ALP*. The relative gene expression (fold change) was normalized to the respective static controls at day 3 and day 7 (baseline). **significant difference ($p<0.05$) between CT and OF vibrations, #significantly changed ($p<0.05$) versus the respective static controls, +significantly different ($p<0.05$) between day 3 and day 7 under corresponding vibration mode.

baseline level, and the OF treatment was found to be more inductive at day 3. The OF treatment was also more inductive toward osteogenesis, as evidenced by the upregulation of *ALP* expression relative to the CT cultures at day 3 and day 7. However, the overall mRNA level of *ACAN*, *ALP*, and *aP2* (undetectable by qPCR, data not shown) was not altered significantly between the static and the dynamic cultures at day 7.

Cellular response at the protein level. In addition to qPCR evaluations at the transcriptional level, important ECM proteins were further quantified biochemically at the protein level (Fig. 10). First, elastin production was characterized by separately analyzing the soluble elastin precursors and the insoluble mature elastin. The deposition of insoluble elastin on the PCL scaffolds under both vibration modes was slightly enhanced relative to the static controls (Fig. 10A). When normalized to the static controls, insoluble elastin production at day 7 of CT (8.54 ± 1.28 μg/mg dry scaffold) and OF (7.49 ± 1.0 μg/mg) vibrations was increased by a fold of 1.33 ± 0.11 and 1.26 ± 0.06 (Supplementary Fig. S2A), respectively. The amount of newly synthesized soluble elastin reached 3.72 ± 0.10 μg/mg and 4.2 ± 0.1 μg/mg after 7 days of CT and OF cultures, respectively, both of which were significantly higher ($p<0.03$) than the static control (42.72 ± 0.21 μg/mg) (Fig. 10B). The secretion of soluble elastin precursors under vibrations was significantly ($p=0.02$) promoted relative to the static controls. Specifically, a fold increase of 1.32 ± 0.08 for the CT treatment and 1.53 ± 0.05 for the OF treatment was detected (Supplementary Fig. S2B).

Cells exposed to 7-day CT treatment produced an average of 4.29 ± 0.39 μg/mg (Fig. 10C) HA, 1.63 ± 0.02 (Supplementary Fig. S2C) times higher than those cultured in the absence of vibratory stimulations. Interestingly ($p=0.02$), HA production after 7-day OF culture (5.95 ± 0.44 μg/mg, Fig. 10C) was 2.16 ± 0.13 (Supplementary Fig. S2C) times higher than the static controls. High-frequency vibratory stimulations significantly enhanced the ability of MSCs to synthesize TNC (Fig. 10D). The TNC production after 7 days of dynamic culture reached an average of 87.12 ± 15.31 ng/mg and 131.36 ± 7.68 ng/mg for CT and OF cultures, respectively, and both of them were markedly higher ($p<0.01$) than the static control (15.73 ± 1.76 ng/mg). Compared with the static controls, it was elevated by 8.98 ± 0.61 fold within 7 days of OF vibrations, which was significantly higher ($p=0.006$) than that of the CT vibrations (5.06 ± 0.51-fold, Supplementary Fig. S2D). The MMP1 synthesis was also dramatically enhanced on vibration (Fig. 10E and Supplementary Fig. S2E). Seven-day CT and OF treatment gave rise to a significant ($p<0.05$) increase in MMP1 secretion relative to the static controls, with a fold increase of 2.42 ± 0.60 and 4.66 ± 0.71, respectively. Cumulatively, the amount of MMP1 produced in OF cultures (175.94 ± 42.62 pg/mg) was higher than in CT cultures (132.62 ± 24.84 pg/mg, Fig. 10E).

Discussion

Mature vocal fold LP is compositionally, structurally, and mechanically different from the new-born tissues.[5] We hypothesize that functional vocal fold tissues can be recreated *in vitro*, via a well-defined tissue engineering strategy, if the vocal fold-like microenvironment is recapitulated. Electrospun PCL meshes were employed to recapitulate the structure of the vocal fold ligament. The micron-sized PCL fibers entangle to form a mesh-like network with inter-fiber spacing that is comparable to the size of individual MSCs. The nanoscale surface texture on individual fibers (created by the condensed droplets of atmospheric water during electrospinning[35]) is likely to provide additional contact guidance, facilitating the initial cell attachment during the 3-day preculture. MSCs formed direct contact with the FN-coated fibers and penetrated into the scaffolds. The establishment of a defined focal adhesion complex ensures the direct coupling of intracellular machinery with the extracellular milieu.[31]

It is generally recognized that the structure and function of tissues and organs reflect the acting physical forces, with profound interactive effects.[36] While the PCL scaffold provided a ligament-like structural support, the vocal fold bioreactor imposed physiologically relevant mechanical signals to the cultured MSCs. The bioreactor employed in this study creates the vibration electromagnetically and transfers the energy aerodynamically to the cultured MSCs, mimicking the natural phonation process in which the vocal folds are

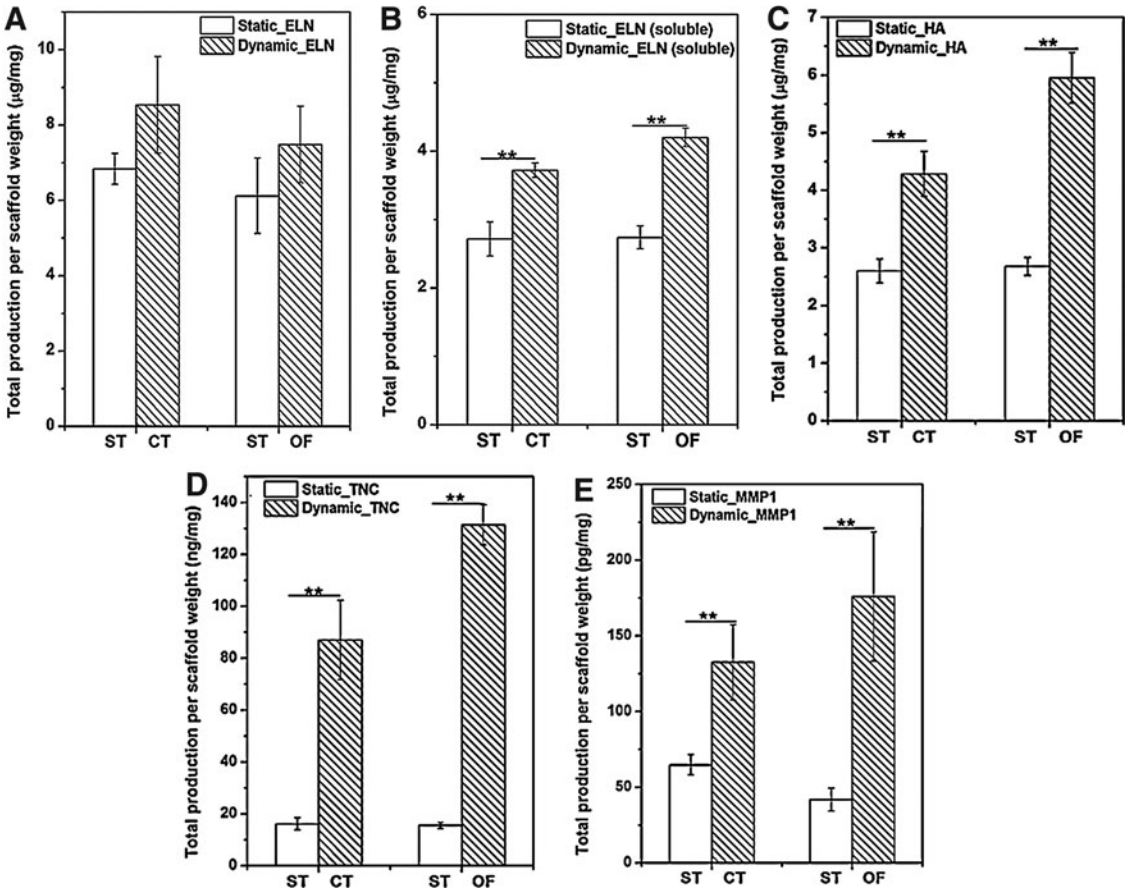

FIG. 10. Biochemical quantification of ELN **(A:** insoluble; **B:** soluble**)**, HA **(C)**, TNC **(D)** and MMP1 **(E)** produced by MSCs cultured on/in the PCL scaffolds under static (ST), CT and OF vibration conditions. Total amount of protein per dry scaffold weight was represented as mean ± SEM, $n = 4$ from the representative trial. $^{**}p < 0.05$: significant difference between the static and dynamic culture.

driven into motion by the air from the lung. Compared with our previous bioreactor design,[23] the current system employs individually fitted vibration chambers, allowing for a significantly larger displacement and a higher acceleration to be achieved, at the same time, minimizing system variations and mechanical perturbation across different vibration units. To accommodate the cellular constructs for 3D dynamic cultures, a centrally positioned, narrow groove was created in the silicone disk so that the scaffolds can be peripherally anchored and tightly secured in the vibration chamber. The geometry of the groove is adjustable; thus, the shape of the construct can be tuned accordingly to better represent the dimension of native vocal folds.[20] Our LDV results confirmed that the sinusoidal signals generated by the function generator were captured by the PCL scaffold or the silicone disk with high fidelity, both oscillating longitudinally in an axisymmetrical manner. Of note, the vibration patterns detected on the disk and the scaffold essentially overlap with each other, confirming that the cellular constructs are not being dislodged during the dynamic study. During normal phonation, a greater subglottal pressure results in higher amplitudes of lateral vocal fold displacement,[2] whereas a higher phonation frequency gives rise to a smaller displacement.[2,20] These characteristics have been recaptured in our vocal fold bioreactor, with w_0 dependent on both f and V_{pp}. Overall, the current vibration device is modular and user friendly, allowing dynamic cell culture studies to be conducted in a high throughput and reproducible fashion. Nevertheless, we acknowledge that the relatively small vibration amplitude attainable is the major limitation of this device. Furthermore, our bioreactor does not recapitulate all mechanical aspects of human phonation. For example, the bioreactor does not simulate the bilateral collision of vocal folds during normal phonation. We are currently designing our third generation of vocal fold bioreactor that will likely overcome these limitations.

MSCs cultivated on/in the PCL scaffolds were subjected to CT or OF vibration regimes for approximately 7 days. In the CT treatment, cells were exposed to a continuous 12 h vibration daily; whereas in the OF treatment, cells received a net total of 6 h vibration daily. The OF vibrations over a period of several hours per day were selected to reproduce the normal speaking conditions.[37] The CT mode was selected to simulate the extreme phonation conditions of heavy voice users such as teachers and professional singers.[20] The vibration conditions employed here neither compromised cell metabolism, viability, or proliferative potentials, nor induced apoptotic responses from the cells, as evidenced by the qPCR results for *p53*.[38] Therefore, unlike previously reported vocal fold bioreactors that induced a significant reduction in cell

viability,[20,39] ours does not introduce any physiological trauma to the cells.

The bioreactor, combined with the fibrous scaffold, was further explored for the creation of vocal fold-like niches to modulate MSC functions. Our initial investigations were directed toward the identification of transmembrane proteins that are central for cellular responses to vibratory signals. It is well known that integrins serve not only as a matrix binding receptor but also as a bi-directional (inside-out signaling and outside-in signaling) mechanosensor that coordinates mechanical-biochemical couplings in and out of the cells.[40–42] The significant augmentation of *ITGA5* at the transcriptional level after 7 days of CT and OF vibrations implies that the vibration-induced MSCs response was integrin mediated. This was further confirmed by the immunostaining results for $\alpha_5\beta_1$ integrin. Particularly, 7-day CT vibrations led to an increased expression of integrin $\alpha_5\beta_1$. The inductive effect on integrin $\alpha_5\beta_1$ was less pronounced in OF groups, possibly due to the periodic relaxation during the 1 h-off phase that weakened the vibrational stress. The observed reinforcement of actin filaments by MSCs cultured under both CT and OF conditions suggests that cells adapt to the vibrational forces through actin polymerization and rearrangement.[41] Since the cytoskeleton actin filaments are mainly linked to the cytoplasmic tail of β_1 integrin receptors via the focal adhesion complex,[43] the F-actin staining results reinforced the notion that MSCs perceive the high-frequency vibratory signals through integrins. Overall, our results suggest that MSCs dynamically cultivated in the fibrous scaffolds respond to the vibratory stimulations via integrin-mediated signaling pathways. The specific molecular mechanism, however, is out of the scope of the current investigation.

Compositionally and structurally, mature vocal fold LP differs significantly from that of newborns. The newborn vocal fold LP is homogenous and mainly constituted of ground substance, glycoproteins, and limited fibrous proteins. By contrast, the adult vocal fold LP is a stratified organization that is abundant in various contents of fibrous proteins (collagen, elastin), structural glycoproteins, proteoglycans, and GAGs in different LP layers.[3,8] Our study confirmed the regulatory roles that high-frequency vibrations exert on the cultured MSCs. The stimulatory effects on cellular expression of *FN*, one of the major proteoglycans found in vocal fold LP, is time- and vibration pattern dependent, with the 7-day routine and OF mode being more conducive than other stimulatory conditions. Elastin is one of the major structural proteins found in vocal fold LP, providing the tissue with extensibility and elasticity that are indispensable for voice production.[44] In our study, the OF vibrations induced a >2-fold increase in elastin expression at the mRNA level and a >1.5-fold enhancement at the protein level for soluble elastin precursors at day 7. Compared with the CT treatment, the OF vibrations are more inductive toward elastogenesis. Cyclic stretch-induced elastin production by smooth muscle cells has been previously reported.[14] However, to our knowledge, this is the first reported case showing a significant enhancement in elastin expression by MSCs induced by high frequency vibrations.

Collagens, predominately collagen I and III, make up 43.4%±2.6% of human LP total proteins.[45] Collagen III, the major component of reticular fibers,[46] and collagen I, in the form of microscopic, bundled fibers, together provide the structural maintenance and viscoelasticity of the vibrating vocal fold tissues.[3,45] Our qPCR analyses revealed similar gene expression patterns for *Col3A1* and *ProCol I*, both of which are significantly attenuated (relative to the static controls) after 3 days of CT vibrations and both of which respond more positively to the OF treatments. This similarity agrees with previous findings showing that collagen type I and III were in close association.[47] Moreover, the gene expression of *LOX*, a key extracellular enzyme responsible for collagen and elastin crosslinking,[48] was also significantly up-regulated under OF conditions. Therefore, vibration-induced promotion of ECM biosynthesis occurred not only at the transcriptional level, but also at the post-translational level. Of note, immunohistochemical analyses (data not shown) for collagen I and collagen III did not reveal any significant vibration-induced alterations at the protein level. The short duration of our dynamic treatments may not be sufficient to elicit cumulative changes of collagen deposition. Alternatively, the rapid degradation of newly synthesized collagens by MMPs may have offset their net accumulations. The latter hypothesis is highly likely, considering the fact that MMP1 is the most differentially regulated ECM enzyme: A >16-fold increase at the mRNA level and a >4-fold increase at the protein level were detected after 7 days of OF treatments. MMP1 is primarily involved in matrix turnover and tissue remodeling.[49] Our results are in agreement with previous results on vibration-induced up-regulation of *MMP1* expression by cells entrapped in an HA matrix.[39] Therefore, cells may respond universally to the vibrational stresses by promoting their catabolic activities and accelerating the ECM turnover, regardless of the surrounding scaffolds and cell types.

Tenascin-C is an important mechanoresponsive glycoprotein that is rich in stress-bearing tissues.[50] Our results show that the *TNC* expression after 7 days of vibrations was dramatically increased, at both the gene and protein levels, with the OF vibrations being more conducive than the CT conditions. This finding is consistent with previous studies with regard to the 3D dynamic culture of MSCs in the presence of cyclic tensile strains.[14,18] It is speculated that when exposed to external mechanical strains, the cells tend to elevate TNC secretion to establish a sliding mechanism and to loosen their contact with their surrounding matrices.[50,51] Another mechanosensitive gene, *COX2*, is generally accepted as a pro-inflammatory indicator. Yang *et al.* found that the low-frequency cyclic stretch on tendon fibroblasts acted synergistically with IL-1β to induce *COX2* gene expression, and this effect was stretch magnitude dependent.[52] Our qPCR results revealed that the expression of *COX2* was significantly up-regulated after 7 days of vibrations, most dramatically under the OF regime. COX2's close association with MMP1 in wound healing and other pathological processes[53,54] explains its similar sensitivity to vibratory cues as MMP1.

HA and DCN are crucial interstitial ECM components that exist predominately in vocal fold SLP. They play critical roles in vocal fold wound healing by maintaining a proper tissue viscoelasticity, assisting collagen assembly, and inhibiting fibrosis or preventing scar formation.[9,55] We discovered that HA and DCN biosynthesis is sensitive to vibrations. Both *HAS1* and *HAS3* expression were elevated after 7 days of vibrations, and this was confirmed by the HA ELISA results

showing an increased HA production for the dynamic cultures, with the OF mode being more effective. Therefore, high-frequency vibrations, especially with OF mode, may offer an efficacious strategy for enhancing the cellular production of HA *in vitro*. On the other hand, 7 days of CT culture suppressed the *DCN* expression significantly. This reduction may result in an attenuation of collagen fibril assembly, which is important for inhibiting scar formation.[55]

Finally, we assessed the differentiation potentials of MSCs that were cultured dynamically in 3D fibrous scaffolds. It is widely acknowledged that the manipulation of stem cell niches, particularly the mechanical microenvironment, is an effective approach to guide stem cell fate selection.[56] Much effort has been focused on applying physiologically relevant mechanical stimulations on MSCs to induce their tissue-specific lineage commitment.[14] Most attempts so far were targeted at tendon/ligament, cartilage, or bone tissues, using cyclic stretch, compression, hydrostatic pressure, or fluid shear.[14] There are relatively fewer studies focusing on high-frequency dynamic culture of stem cells for vocal fold tissue engineering purposes.[22] One of our goals was to coax MSCs to adapt PVFF-like behaviors. Our qPCR analyses for typical markers (alkaline phosphatase, aggrecan, *aP2*, and *αSMA*) of alternative MSCs differentiation pathways confirm that the potential of the classic osteoblastic, chondrogenic, adipogenic,[11,57] and myofibroblastic differentiation[19] was not elicited significantly after 7 days of dynamic culture. Considering procollagen I, collagen III, fibronectin, tenascin-C, and MMP1 as the broad fibroblastic hallmarks,[58] it is clear that the high-frequency vibratory stimulations applied in this study, especially the OF mode, promote the fibroblastic commitment of MSCs. Unfortunately, no exclusive marker for vocal fold fibroblasts or vocal fold-specific ECM has been identified so far.[12,58] Future efforts that identify the specific matrix or cellular markers of human vocal folds are certainly needed to improve the outcome of vocal fold regeneration using stem cell and tissue engineering strategies.

Conclusion

Physiologically relevant high-frequency vibrations, combined with a 3D cell culture system, were employed to simulate the microenvironment of vibrating human vocal folds. The fibrous scaffolds containing adhering MSCs were subjected to sinusoidal vibrations continuously or intermittently in a 1-h-on-1-h-off pattern at 200 Hz with a normal displacement (at the center of the constructs) of 40 μm for up to 7 days. The vibration regimens applied did not induce any significant physiological trauma to the cultured MSCs. Cells were actively engaged in the production and remodeling of vocal fold-like ECM. Overall, the OF mode is more efficient in eliciting the desired cellular responses, and the integrin-mediated mechanotransduction mechanism may contribute to the vibration-induced responses. Overall, the vibratory stimulations promoted MSCs to adopt the behaviors of vocal fold fibroblasts. Our findings underscore the significance of physiologically relevant mechanical loadings in modulating stem cell behaviors for the *in vitro* engineering of functional vocal fold tissues.

Acknowledgments

The authors thank Dr. Jeffrey Caplan for his training and advice on confocal imaging. They also thank the Keck Electron Microscopy Lab and Dr. Chaoying Ni and Mr. Frank Kriss for SEM assistance. This work is funded by National Institutes of Health (NIDCD, R01 008965 and R01DC011377).

Disclosure Statement

No competing financial interests exist.

References

1. Titze, I.R. Mechanical-stress in phonation. J Voice **8,** 99, 1994.
2. Titze, I.R. On the relation between subglottal pressure and fundamental-frequency in phonation. J Acoust Soc Am **85,** 901, 1989.
3. Gray, S.D. Cellular physiology of the vocal folds. Otolaryngol Clin North Am **33,** 679, 2000.
4. Thibeault, S.L., Gray, S.D., Bless, D.M., Chan, R.W., and Ford, C.N. Histologic and rheologic characterization of vocal fold scarring. J Voice **16,** 96, 2002.
5. Hartnick, C.J., Rehbar, R., and Prasad, V. Development and maturation of the pediatric human vocal fold lamina propria. Laryngoscope **115,** 4, 2005.
6. Ishii, K., Yamashita, K., Akita, M., and Hirose, H. Age-related development of the arrangement of connective tissue fibers in the lamina propria of the human vocal fold. Ann Otol Rhinol Laryngol **109,** 1055, 2000.
7. Newman, S.R., Butler, J., Hammond, E.H., and Gray, S.D. Preliminary report on hormone receptors in the human vocal fold. J Voice **14,** 72, 2000.
8. Sato, K., and Hirano, M. Histologic investigation of the macula flava of the human newborn vocal fold. Ann Otol Rhinol Laryngol **104,** 556, 1995.
9. Branski, R.C., Verdolini, K., Sandulache, V., Rosen, C.A., and Hebda, P.A. Vocal fold wound healing: A review for clinicians. J Voice **20,** 432, 2006.
10. Hansen, J.K., and Thibeault, S.L. Current understanding and review of the literature: vocal fold scarring. J Voice **20,** 110, 2006.
11. Pittenger, M.F., Mackay, A.M., Beck, S.C., Jaiswal, R.K., Douglas, R., Mosca, J.D., *et al.* Multilineage potential of adult human mesenchymal stem cells. Science **284,** 143, 1999.
12. Hanson, S.E., Kim, J., Johnson, B.H.Q., Bradley, B., Breunig, M.J., Hematti, P., *et al.* Characterization of mesenchymal stem cells from human vocal fold fibroblasts. Laryngoscope **120,** 546, 2010.
13. Jones, D.L., and Wagers, A.J. No place like home: anatomy and function of the stem cell niche. Nat Rev Mol Cell Biol **9,** 11, 2008.
14. Wang, J. H.C., and Thampatty, B.P. Mechanobiology of Adult and Stem Cells. International Review of Cell and Molecular Biology, vol 271. San Diego: Elsevier Academic Press, Inc., 2008, p. 301.
15. Iqbal, J., and Zaidi, M. Molecular regulation of mechanotransduction, Biochemical and Biophysical Research Communications **328,** 751, 2005.
16. Kim, B.S., Nikolovski, J., Bonadio, J., and Mooney, D.J. Cyclic mechanical strain regulates the development of engineered smooth muscle tissue. Nat Biotechnol **17,** 979, 1999.
17. Webb, K., Hitchcock, R.W., Smeal, R.M., Li, W.H., Gray, S.D., and Tresco, P.A. Cyclic strain increases fibroblast proliferation, matrix accumulation, and elastic modulus of fibroblast-seeded polyurethane constructs. J Biomech **39,** 1136, 2006.
18. Doroski, D.M., Levenston, M.E., and Temenoff, J.S. Cyclic tensile culture promotes fibroblastic differentiation of

marrow stromal cells encapsulated in poly(ethylene glycol)-based hydrogels. Tissue Eng Part A **16,** 3457, 2010.
19. Tong, Z., and Jia, X. Biomaterial-based strategies for the engineering of mechanically active soft tissues. MRS Commun **2,** 31, 2012.
20. Titze, I.R., Hitchcock, R.W., Broadhead, K., Webb, K., Li, W., Gray, S.D., *et al.* Design and validation of a bioreactor for engineering vocal fold tissues under combined tensile and vibrational stresses. J Biomech **37,** 1521, 2004.
21. Kutty, J.K., and Webb, K. Vibration stimulates vocal mucosa-like matrix expression by hydrogel-encapsulated fibroblasts. J Tissue Eng Regen M **4,** 62, 2010.
22. Gaston, J., Rios, B.Q., Bartlett, R., Berchtold, C., and Thibeault, S.L. The response of vocal fold fibroblasts and mesenchymal stromal cells to vibration. Plos One **7,** 2012.
23. Farran, A.J.E., Teller, S.S., Jia, F., Clifton, R.J., Duncan, R.L., and Jia, X. Design and characterization of a dynamic vibrational culture system. J Tissue Eng Regen Med **7,** 213, 2013.
24. Bianco, P., and Robey, P.G. Stem cells in tissue engineering. Nature **414,** 118, 2001.
25. Tong, Z., Sant, S., Khademhosseini, A., and Jia, X. Controlling the fibroblastic differentiation of mesenchymal stem cells via the combination of fibrous scaffolds and connective tissue growth factor. Tissue Eng Part A **17,** 2773, 2011.
26. Bustin, S.A., Benes, V., Garson, J.A., Hellemans, J., Huggett, J., Kubista, M., *et al.* The miqe guidelines: Minimum information for publication of quantitative real-time pcr experiments. Clin Chem **55,** 611, 2009.
27. Dingemans, A.-M., van den Boogaart, V., Vosse, B., van Suylen, R.-J., Griffioen, A., and Thijssen, V. Integrin expression profiling identifies integrin alpha5 and beta1 as prognostic factors in early stage non-small cell lung cancer. Mol Cancer **9,** 152, 2010.
28. Fink, T., Lund, P., Pilgaard, L., Rasmussen, J., Duroux, M., and Zachar, V. Instability of standard pcr reference genes in adipose-derived stem cells during propagation, differentiation and hypoxic exposure. BMC Mol Biol **9,** 98, 2008.
29. Vandesompele, J., De Preter, K., Pattyn, F., Poppe, B., Van Roy, N., De Paepe, A., *et al.* Accurate normalization of real-time quantitative rt-pcr data by geometric averaging of multiple internal control genes. Genome Biol **3,** 12, 2002.
30. Hellemans, J., Mortier, G., De Paepe, A., Speleman, F., and Vandesompele, J. Qbase relative quantification framework and software for management and automated analysis of real-time quantitative pcr data. Genome Biol **8,** R19, 2007.
31. Critchley, D.R. Cytoskeletal proteins talin and vinculin in integrin-mediated adhesion. Biochem Soc Trans **32,** 831, 2004.
32. Sapozhnikov, O.A., Morozov, A.V., and Cathignol, D. Piezoelectric transducer surface vibration characterization using acoustic holography and laser vibrometry. Presented at the Ultrasonics Symposium, 2004 IEEE, Montreal, Canada.
33. Brown, W.S., Morris, R.J., Hollien, H., and Howell, E. Speaking fundamental-frequency characteristics as a function of age and professional singing. J Voice **5,** 310, 1991.
34. Katsumi, A., Orr, A.W., Tzima, E., and Schwartz, M.A. Integrins in mechanotransduction. J Biol Chem **279,** 12001, 2004.
35. Megelski, S., Stephens, J.S., Chase, D.B., and Rabolt, J.F. Micro- and nanostructured surface morphology on electrospun polymer fibers. Macromolecules **35,** 8456, 2002.
36. Ingber, D.E. Cellular mechanotransduction: putting all the pieces together again. Faseb J **20,** 811, 2006.
37. Masuda, T., Ikeda, Y., Manako, H., and Komiyama, S. Analysis of vocal abuse - fluctuations in phonation time and intensity in 4 groups of speakers. Acta Oto-Laryngol **113,** 547, 1993.
38. Itahana, K., Dimri, G.P., Hara, E., Itahana, Y., Zou, Y., Desprez, P.Y., *et al.* A role for p53 in maintaining and establishing the quiescence growth arrest in human cells. J Biol Chem **277,** 18206, 2002.
39. Kutty, J.K., and Webb, K. Tissue engineering therapies for the vocal fold lamina propria. Tissue Eng Part B Rev **15,** 249, 2009.
40. Kim, M., Carman, C.V., and Springer, T.A. Bidirectional transmembrane signaling by cytoplasmic domain separation in integrins. Science **301,** 1720, 2003.
41. Ross, R.S. Molecular and mechanical synergy: cross-talk between integrins and growth factor receptors. Cardiovasc Res **63,** 381, 2004.
42. Clark, E.A., and Brugge, J.S. Integrins and signal-transduction pathways - the road taken. Science **268,** 233, 1995.
43. Friedland, J.C., Lee, M.H., and Boettiger, D. Mechanically activated integrin switch controls alpha(5)beta(1) function. Science **323,** 642, 2009.
44. Moore, J., and Thibeault, S. Insights into the role of elastin in vocal fold health and disease. J Voice **26,** 269.
45. Hahn, M.S., Kobler, J.B., Zeitels, S.M., and Langer, R. Quantitative and comparative studies of the vocal fold extracellular matrix ii: Collagen. Ann Otol Rhinol Laryngol **115,** 225, 2006.
46. Sato, K. Reticular fibers in the vocal fold mucosa. Ann Otol Rhinol Laryngol **107,** 1023, 1998.
47. Cleutjens, J.P.M., Verluyten, M.J.A., Smits, J.F.M., and Daemen, M.J.A.P. Collagen remodeling after myocardial-infarction in the rat-heart. Am J Pathol **147,** 325, 1995.
48. Kagan, H.M., and Sullivan, K.A. Lysyl oxidase - preparation and role in elastin biosynthesis. Methods Enzymol **82,** 637, 1982.
49. Clark, I.A., Swingler, T.E., Sampieri, C.L., and Edwards, D.R. The regulation of matrix metalloproteinases and their inhibitors. Int J Biochem Cell Biol **40,** 1362, 2008.
50. Chiquet, M., Gelman, L., Lutz, R., and Maier, S. From mechanotransduction to extracellular matrix gene expression in fibroblasts. Biochim Biophys Acta-Mol Cell Res **1793,** 911, 2009.
51. Chiquetehrismann, R., Kalla, P., Pearson, C.A., Beck, K., and Chiquet, M. Tenascin interferes with fibronectin action. Cell **53,** 383, 1988.
52. Yang, G.G., Im, H.J., and Wang, J.H.C. Repetitive mechanical stretching modulates il-1 beta induced cox-2, mmp-1 expression, and pge(2) production in human patellar tendon fibroblasts. Gene **363,** 166, 2005.
53. Christofori, G. Cancer: division of labour. Nature **446,** 735, 2007.
54. Gilroy, D.W., Saunders, M.A., and Wu, K.K. Cox-2 expression and cell cycle progression in human fibroblasts. Am J Physiol-Cell Physiol **281,** C188, 2001.
55. Thibeault, S.L., Bless, D.M., and Gray, S.D. Interstitial protein alterations in rabbit vocal fold with scar. J Voice **17,** 377, 2003.
56. Engler, A.J., Sen, S., Sweeney, H.L., and Discher, D.E. Matrix elasticity directs stem cell lineage specification. Cell **126,** 677, 2006.
57. Chamberlain, G., Fox, J., Ashton, B., and Middleton, J. Concise review: Mesenchymal stem cells: Their phenotype, differentiation capacity, immunological features, and potential for homing. Stem Cells **25,** 2739, 2007.

58. Lee, C.H., Shah, B., Moioli, E.K., and Mao, J.J. Ctgf directs fibroblast differentiation from human mesenchymal stem/stromal cells and defines connective tissue healing in a rodent injury model. J Clin Invest **120,** 3340, 2010.
59. Chen, X., and Thibeault, S.L. Biocompatibility of a synthetic extracellular matrix on immortalized vocal fold fibroblasts in 3-d culture. Acta Biomater **6,** 2940, 2010.
60. Guo, N., Li, X., Mann, M.M., Funderburgh, M.L., Du, Y., and Funderburgh, J.L. Hyaluronan synthesis mediates the fibrotic response of keratocytes to transforming growth factor beta. J Biol Chem **285,** 32012.
61. Calabro, A., Oken, M.M., Hascall, V.C., and Masellis, A.M. Characterization of hyaluronan synthase expression and hyaluronan synthesis in bone marrow mesenchymal progenitor cells: predominant expression of has1 mrna and upregulated hyaluronan synthesis in bone marrow cells derived from multiple myeloma patients. Blood **100,** 2578, 2002.
62. Kurpinski, K., Chu, J., Hashi, C., and Li, S. Anisotropic mechanosensing by mesenchymal stem cells. Proc Natl Acad Sci U S A **103,** 16095, 2006.
63. O'Brien, M., O'Shaughnessy, D., Ahamide, E., Morrison, J.J., and Smith, T.J. Differential expression of the metalloproteinase mmp3 and the alpha 5 integrin subunit in human myometrium at labour. Mol Hum Reprod **13,** 655, 2007.
64. Syeda, F., Grosjean, J., Houliston, R.A., Keogh, R.J., Carter, T.D., Paleolog, E., *et al.* Cyclooxygenase-2 induction and prostacyclin release by protease-activated receptors in endothelial cells require cooperation between mitogen-activated protein kinase and nf-kappa b pathways. J Biol Chem **281,** 11792, 2006.
65. Fang, Y.Y., and Svoboda, K.K.H. Nicotine inhibits myofibroblast differentiation in human gingival fibroblasts. J Cell Biochem **95,** 1108, 2005.
66. Chen, S.B., Takanashi, S.C., Zhang, Q.S., Xiong, W., Zhu, S.T., Peters, E.C., *et al.* Reversine increases the plasticity of lineage-committed mammalian cells. Proc Natl Acad Sci U S A **104,** 10482, 2007.
67. Curtis, K.M., Gomez, L.A., Rios, C., Garbayo, E., Raval, A.P., Perez-Pinzon, M.A., *et al.* Ef1 alpha and rpl13a represent normalization genes suitable for rt-qpcr analysis of bone marrow derived mesenchymal stem cells. BMC Mol Biol **11,** 15.
68. Boone, D.N., Qi, Y., Li, Z., and Hann, S.R. Egr1 mediates p53-independent c-Myc-induced apoptosis via a non-canonical arf-dependent transcriptional mechanism. Proc Natl Acad Sci **108,** 632.

Address correspondence to:
Xinqiao Jia, PhD
Department of Materials Science and Engineering
Delaware Biotechnology Institute
Biomedical Engineering Program
201 DuPont Hall
University of Delaware
Newark, DE 19716

E-mail: xjia@udel.edu

Received: November 21, 2012
Accepted: March 8, 2013
Online Publication Date: April 25, 2013